RSC Advances

PAPER

View Article Online
View Journal | View Issue

Cite this: *RSC Adv.*, 2021, **11**, 17891

Kinetic and deuterium isotope analyses of ammonia electrochemical synthesis†

Chien-I. Li, [a] Hiroki Matsuo [b] and Junichiro Otomo *[b]

The mechanism of electrochemical promotion of ammonia formation was investigated by kinetic and deuterium isotope analyses using a cell with a Pt (anode)|$BaCe_{0.9}Y_{0.1}O_3$ (BCY)|Fe (cathode) configuration on the introduction of a gaseous mixture of $H_2(D_2)$–N_2 to the cathode at 550 °C. To clarify the mechanism of electrochemical ammonia synthesis, the reaction orders for hydrogen, α, and nitrogen, β, were investigated. The values of α and β did not change after applying a negative voltage, which indicates that the reaction mechanism at rest potential is the same as that with cathodic polarization. Furthermore, deuterium isotope analysis was conducted to investigate the mechanism of electrochemical promotion. The isotopic composition of ammonia (*i.e.*, $NH_{3-x}D_x$) formed in the cathode was determined using Fourier-transform infrared spectroscopy (FTIR). The results show that the ammonia products with cathodic polarization correspond to the species of H_2 (or D_2) in the cathode, that is, NH_3 (or ND_3) was mainly formed when H_2 (or D_2) was introduced to the cathode. Isotopic analysis revealed that the ammonia formation rate *via* the electrochemical promotion of catalysis (EPOC) is faster than that *via* the charge-transfer reaction, suggesting that a significant increase in the ammonia formation rate will be caused by the EPOC.

Received 9th January 2021
Accepted 3rd May 2021

DOI: 10.1039/d1ra00190f

rsc.li/rsc-advances

Introduction

Ammonia is an essential chemical, and approximately 140 million tons of ammonia are synthesized each year.[1] Most of the produced ammonia is used as a fertilizer in agriculture to produce foodstuffs and feed the world's population.[2] In the past century, as the world population has more than tripled, the demand for nitrogen fertilizer and ammonia has also increased significantly.[2] In addition, ammonia is a potential hydrogen carrier because of its advantages, such as its high hydrogen density of 17.8%, ease of storage and transport, and emission of only N_2 and H_2O on combustion; thus, it could form an important part of the hydrogen economy.[3–5]

Currently, ammonia is produced industrially by the Haber–Bosch process, in which N_2 and H_2 are reacted together at high pressure (150–200 bar) and temperature (400 °C) on an iron-based catalyst to produce NH_3.[6,7] Normally, the rate-determining step on an Fe catalyst is considered to be N_2 dissociation because of the high strength of the N≡N triple bond. It has been reported that the N_2 dissociation reaction can be accelerated by the addition of K_2O or Al_2O_3 to the Fe-based catalyst. This increases the ammonia synthesis activity[8] because the K additive has a low work function and can promote electron back-donation reaction from Fe into the $N_2\pi^*_{2p}$ orbital.[9] On the other hand, Ru catalysts show better activity in ammonia synthesis than Fe catalysts.[6,7] Aika *et al.* compared the ammonia synthesis activity of different alkali metal additives as promoters in Ru or Ni-based catalysts. They concluded that Cs had a stronger promoting effect than K or Na.[9] On the other hand, Kitano *et al.* also observed a high ammonia formation rate (46.41 μg mg^{-1} h^{-1}) using a Ru-loaded $12CaO{-}7Al_2O_3$ electride.[10,11] They proposed that electron back-donation from the electride to the $N_2\pi^*_{2p}$ orbital facilitates N_2 dissociation and accelerates the ammonia formation rate.

However, the Haber–Bosch process is energy-intensive and releases large amounts of carbon dioxide because methane reforming is used to produce the required hydrogen. Therefore, to reduce carbon emissions and energy consumption during ammonia synthesis, a more environmentally friendly process, such as an electrochemical route, has been developed. This process allows more efficient NH_3 formation at moderate pressures and temperatures.

Over the last two decades, the electrosynthesis of ammonia from H_2O and N_2 has attracted great attention because this process can achieve high energy and current efficiencies.[12] In ammonia electrosynthesis using a proton conductor, H_2O is decomposed to H^+, e^-, and O_2 in the anode (eqn (1)), and the H^+ ions pass through the electrolyte to react with N_2 and e^- in the cathode (eqn (2)). The overall reaction is presented in eqn (3); as can be seen, it is a carbon-free process. In non-aqueous systems,

[a]*Department of Environment Systems, Graduate School of Frontier Sciences, The University of Tokyo, 5-1-5 Kashiwanoha, Kashiwa-shi, Chiba 277-8563, Japan*
[b]*Department of Transdisciplinary Science and Engineering, School of Environment and Society, Tokyo Institute of Technology, 2-12-1 Ookayama, Meguro-ku, Tokyo 152-8550, Japan. E-mail: otomo.j.aa@m.titech.ac.jp*

† Electronic supplementary information (ESI) available. See DOI: 10.1039/d1ra00190f

to improve the N_2 reduction activity, H_2O is replaced by H_2 as the proton source in the anode.

Anode:

$$H_2O \rightarrow \frac{1}{2}O_2 + 2H^+ + 2e^- \quad (1)$$

Cathode:

$$N_2 + 6H^+ + 6e^- \rightarrow 2NH_3 \quad (2)$$

Overall:

$$N_2 + 3H_2O \rightarrow 2NH_3 + \frac{3}{2}O_2 \quad (3)$$

At low temperatures (<100 °C), the direct dissociation of N_2 over the catalyst cannot proceed because of the sluggish reaction kinetics. Using density functional theory (DFT) calculations, Skulason *et al.* proposed an alternative route for the protonation of N_2 *via* a charge transfer reaction to form NH_3.[13] The protons supplied from the anode acted as the hydrogen source and reacted with N_2 to form NH_3 through N_2H and N_2H_2 intermediates.[13] Further, several studies have reported electrochemical ammonia formation rates of approximately 10^{-11} to 10^{-8} mol cm^{-2} s^{-1} and current efficiencies of 0.7–56% under a pure N_2 atmosphere at temperatures below 100 °C.[14–21]

On the other hand, many researchers have achieved the electrochemical reduction of N_2 by introducing pure N_2 into the cathode at high temperatures (>500 °C) using a variety of catalysts.[22–33] Low ammonia formation rates of 10^{-11} to 10^{-9} mol s^{-1} cm^{-2} have been reported under these conditions.[22–25,28–33] Wang *et al.* proposed that the ammonia formation rate is affected by several factors, including the electrode area, the conductivity of the proton-conducting solid oxide electrolyte, and the N_2 flow rate.[22,29,30,32] At present, the hypothesis that the enhancement of the ammonia formation rate with cathodic polarization is caused by a faradaic reaction (*i.e.*, charge-transfer reaction), in which N_2 reacts with the H^+ supplied from the anode to form ammonia, is generally accepted.

Some previous studies have also investigated the electrosynthesis of ammonia by introducing a gaseous mixture of H_2–N_2 into the cathode.[34–37] Normally, the ammonia formation rate in an H_2–N_2 atmosphere is higher than that in a pure N_2 atmosphere.[35,37] In our previous study,[37] the electrochemical synthesis of ammonia was investigated using a single cell configuration: wet H_2–Ar, Pt|$BaCe_{0.9}Y_{0.1}O_3$ (BCY)|Al–Fe–K–BCY, H_2–N_2. In the experiment, we found that the ammonia formation rate was increased by 20 times to 6×10^{-10} mol s^{-1} cm^{-2} with cathodic polarization compared with that at rest potential using 15% H_2–85% N_2 in the cathode, whereas low ammonia formation rates of $5.5 \times 10^{-12} - 2.4 \times 10^{-11}$ mol cm^{-2} s^{-1} were obtained using pure N_2 in the cathode. Ouzounidou *et al.* also reported the similar result that an ammonia formation rate of 2.2×10^{-10} mol s^{-1} cm^{-2} in H_2–N_2 was higher than that (1.3×10^{-11} mol s^{-1} cm^{-2}) in pure N_2. Notably, they found that the current efficiency of ammonia electrosynthesis was greater than 100% in the H_2–N_2 atmosphere. This result suggests that, in addition to the faradaic reaction, the ammonia formation rate was also increased by the surface reaction of N_2 and H_2 at the cathode with cathodic polarization. That is, a non-faradaic reaction is involved: the so-called electrochemical promotion of catalysis (EPOC), and this can be controlled by controlling the work function to improve reaction rates.[35] However, it is still unclear whether the dominant effect of the electrochemical promotion of ammonia formation is caused by either the faradaic reaction or the EPOC.

In our recent study,[38] we reported the following results: (1) a cathode structure with short triple phase boundary (TPB) length (*i.e.*, porous pure Fe cathode) had better performance of ammonia formation rate than that with long TPB length (*i.e.*, Fe–BCY cermet cathode), (2) the ammonia formation rate had a strong correlation with the H_2 partial pressure in the cathode. The ammonia formation rate increased from 2.2×10^{-9} mol cm^{-2} s^{-1} (71 μg mg^{-1} h^{-1}) in 10% H_2–90% N_2 to 1.4×10^{-8} mol cm^{-2} s^{-1} (450 μg mg^{-1} h^{-1}) in 50% H_2–50% N_2 using porous pure Fe cathode at 550 °C and −1.2 V, which is equivalent to that in the Haber–Bosch process (250–976 μg mg^{-1} h^{-1} at 7–10 MPa and 400 °C).[7] Furthermore, based on the results, we proposed that the promotion of electrochemical ammonia formation is governed by EPOC with porous pure Fe. Here, to examine the electrochemical promotion of ammonia formation, the information of the origin of hydrogen atoms in ammonia is very important. If the hydrogen atoms in ammonia originate from H_2 in the cathode, ammonia formation will be followed by a surface reaction with EPOC (eqn (4)). If the hydrogen atoms in ammonia originate from H^+ from the anode, ammonia formation will proceed *via* the charge-transfer reaction at the TPB among the gas, Fe catalyst, and BCY proton-conductor (eqn (5)).

$$N_2 + 3H_2 \rightarrow 2NH_3 \quad (4)$$

$$N_2 + 6H^+ + 6e^- \rightarrow 2NH_3 \quad (5)$$

In this study, to investigate the mechanism of the electrochemical promotion of ammonia formation, (1) kinetic analysis and (2) isotope deuterium analysis were conducted using a porous pure Fe cathode at high temperature (550 °C). The dependence of the ammonia formation rate on the cathodic polarization was examined. In addition, the reaction mechanism of electrochemical promotion of ammonia formation was investigated in terms of the reaction orders of hydrogen and nitrogen at rest potential and applied voltage. Furthermore, to investigate the origin of the hydrogen (deuterium) atoms in the formed ammonia, deuterium isotope analysis was also performed using Fourier transform infrared (FTIR) spectroscopy measurements at high temperature (550 °C). *Via* the analysis of the hydrogen/deuterium composition of the ammonia ($NH_{3-x}D_x$) formed in the cathode, we discuss which mechanism, that is, the faradaic reaction or EPOC, is dominant for ammonia formation. In our experiments, gaseous mixtures of dry N_2–D_2–Ar and wet H_2–Ar were introduced into the cathode and anode, respectively. If the ammonia were formed by the surface reaction of N_2 with D_2 *via* the EPOC in the cathode, the main

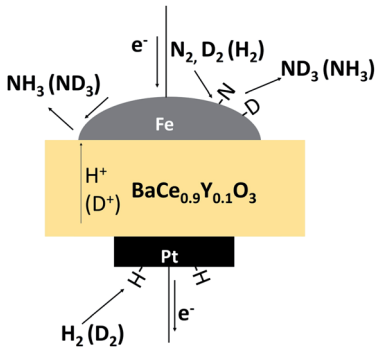

Fig. 1 A schematic image of ammonia formation and deuterium isotope analysis through the observation of ammonia composition, $NH_{3-x}D_x$.

product should be ND_3. In contrast, if the ammonia were formed by the charge-transfer reaction of N_2 with H^+ from the anode, the product should be NH_3, as shown in Fig. 1. To the best of our knowledge, this manuscript is the first study which demonstrates the deuterium isotope analysis for the electrochemical ammonia formation in a solid oxide electrolyzer cell. Furthermore, because of the serious problem of contamination for ammonia electrochemical synthesis, the relevant protocol was suggested with a series of check items.[39] In this study, we also checked the experimental procedure very carefully to avoid the influence of contamination on kinetic and deuterium isotope analyses. Therefore, using our experimental method, we can reveal whether ammonia formation occurs on the surface or at the TPB, and this information will contribute to the design of cathode structures for effective electrochemical reactors.

Results and discussion

Characterizations

Fig. 2 shows the XRD patterns of the porous pure Fe cathodes on the BCY electrolyte. Strong peaks corresponding to the thick BCY electrolyte and peaks corresponding to Fe at 44.46° and 65.02° (cubic, $Im\bar{3}m$, PDF #00-006-0696), respectively, were observed. Fig. 3 shows cross-sectional SEM images of the pure porous Fe cathode. The thickness of the cathode was approximately 30 μm, and the size of the Fe particles ranged from 50 to 500 nm.

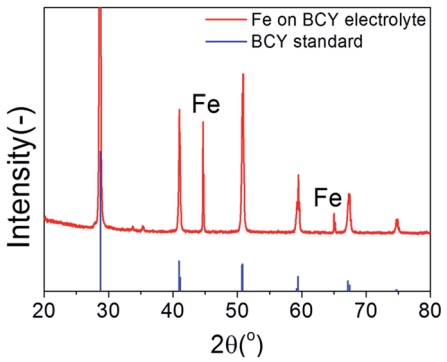

Fig. 2 XRD spectra of porous pure Fe cathode on the BCY electrolyte. Reflections from the BCY standard card (PDF #01-070-1429) are shown in blue.

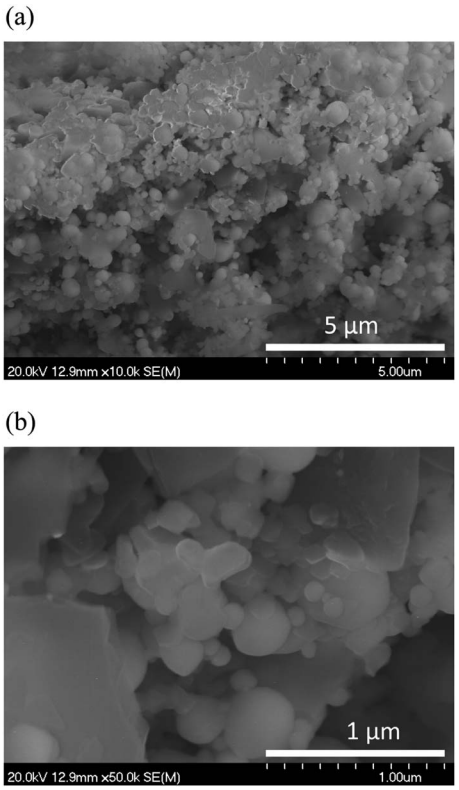

Fig. 3 (a) Cross-sectional SEM images of the as-prepared samples of porous pure Fe cathode. (b) is the enlarged image of the as-prepared samples of porous pure Fe cathode without polishing.

Electrochemical promotion of ammonia formation at different H_2 partial pressures

Fig. 4 shows the ammonia formation rate at different applied voltages using a cell with 20% H_2–3% H_2O–77% Ar (30 sccm), Pt|BCY|Fe, 50% N_2–H_2–Ar (40 sccm). Electrode potentials corresponding to the applied voltages at different atmospheres were listed in the ESI (Table S1†). The ammonia formation rate was evaluated by increasing the H_2 partial pressure (p_{H_2}) from 0.05 to 0.25 atm at rest potential. Furthermore, at an applied voltage of −1.3 V, the ammonia formation rates increased by approximately 3.5–6.5 times compared with those at the rest potential at different H_2 partial pressures. Fig. 4b reveals a slight decrease in the current densities with increasing H_2 partial pressure, which is probably caused by the low overpotential at high H_2 partial pressure because the rest potential is more negative at high H_2 partial pressures than that at low H_2 partial pressures in the cathode.

Fig. 4c shows the $\ln(p_{H_2})$ dependence of $\ln(r_{NH_3})$. The hydrogen partial pressure used for the horizontal axis in Fig. 4c is defined as the sum of the hydrogen partial pressure in the feed gas and that as a result of the H_2 evolution reaction. We assume that the current efficiency of the H_2 evolution reaction is 100% (eqn (6)), which suggests that the H_2 partial pressure in the cathode increases with cathodic polarization (Δp_{H_2} in eqn (7)).

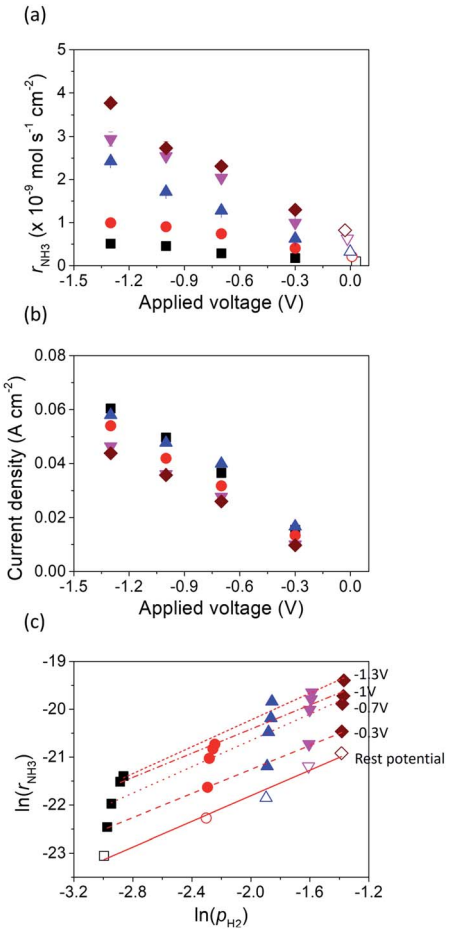

Fig. 4 (a) Ammonia formation rate, (b) current density, and (c) $\ln(r_{NH_3})$ *vs.* $\ln(p_{H_2})$ using porous pure Fe cathode at 550 °C and different H_2 partial pressures. ■ 5% H_2–50% N_2 with cathodic polarization. □ 5% H_2–50% N_2 at rest potential. ● 10% H_2–50% N_2 with cathodic polarization. ○ 10% H_2–50% N_2 at rest potential. ▲ 15% H_2–50% N_2 with cathodic polarization. △ 15% H_2–50% N_2 at rest potential. ▼ 20% H_2–50% N_2 with cathodic polarization. ▽ 20% H_2–50% N_2 at rest potential. ◆ 25% H_2–50% N_2 with cathodic polarization. ◇ 25% H_2–50% N_2 at rest potential.

$$2H^+ + 2e^- \rightarrow H_2(g) \quad (6)$$

$$\Delta p_{H_2} = \frac{i \times A \times R \times T}{n \times F \times f} \quad (7)$$

Here, i, A, R, T, n, F, and f are the current density, electrode area, gas constant, temperature, reaction electron number, Faraday constant, and flow rate in the cathode, respectively. The reaction order for hydrogen, α, was calculated using eqn (8).

$$r_{NH_3} = k p_{H_2}^{\alpha} p_{N_2}^{\beta} \quad (8)$$

where k is the rate constant. α was approximately 1.3 at the rest potential, which is slightly different from that (1.4) obtained using K-promoted Fe catalysts[40] and that (0.69) obtained using the K–Al–Fe–BCY catalyst.[37] Notably, the α values at applied voltages of −0.3, −0.7, −1, and −1.3 V were approximately 1.2–1.4, which are similar to those at the rest potential, as shown in Table 1.

The reaction order of nitrogen was also investigated at a fixed H_2 partial pressure of 0.1 atm and N_2 partial pressures of 0.3–0.6 atm (see Fig. S1†). The influence of increasing the N_2 partial pressure on the ammonia formation rate was very weak because of the low value of β, which was 0.3 at rest potential, smaller than that of 0.96 and 0.52 in previous studies.[37,40] The values of β at different applied voltages are summarized in Table 1. Notably, at the rest potential, neither α nor β change after the application of different voltages, which suggests that the reaction mechanism with cathodic polarization is probably the same as that at the rest potential, that is, a surface reaction. To investigate the details of the reaction mechanism of electrochemical ammonia synthesis, deuterium isotope analysis using FTIR measurements was conducted to examine the origin of the hydrogen atoms in the ammonia product, as discussed in the next section.

Table 1 Values of α and β at different voltages

Applied voltage (V)	α	β
Rest potential	1.33 ± 0.11	0.30 ± 0.15
−0.3	1.26 ± 0.04	0.59 ± 0.09
−0.7	1.38 ± 0.06	0.37 ± 0.25
−1	1.26 ± 0.09	0.43 ± 0.21
−1.3	1.40 ± 0.13	0.56 ± 0.2

FTIR spectra of $NH_{3-x}D_x$

In this study, the ν_2 band (umbrella mode) of $NH_{3-x}D_x$ was investigated. The IR spectra of NH_3 shows two Q branches arising from the splitting of the degenerate energy level[41] (see Section 4 and Fig. S2 in the ESI†). According to the selection rule, the vibrational–rotational transition only occurs from the symmetric state to the asymmetric state or *vice versa*. In addition, the vibrational quantum number, ν, the quantum number for the total angular momentum, J, and the quantum number for the projection of J onto the principal axis of the molecule, K, must satisfy $\Delta\nu = 1$, $\Delta J = \pm 1$, 0, and $\Delta K = 0$. $\Delta J = 0$, 1, and −1 are represented by Q, P, and R branches, respectively, as shown in Fig. S3.† Therefore because of the special molecular shape, motion (that is, umbrella inversion), and the selection rule, NH_3 shows two Q branches at approximately 965 and 930 cm^{-1}. On the other hand, by replacing H atoms with D atoms, the energy difference between the Q branches decreases because of the heavy D atoms. The details of the wavenumbers of the Q, P, and R branches for $NH_{3-x}D_x$ are summarized in Section 5 in the ESI, Tables S3–S8.† In Fig. 5 and 6, only Q branches, which represent the transition from the symmetric to the asymmetric state ($0_s \rightarrow 1_a$), and Q′ branches, which represent the transition from the asymmetric to the symmetric states ($1_s \rightarrow 0_a$) of $NH_{3-x}D_x$ are marked because of their high absorbance. The absorption coefficients of $NH_{3-x}D_x$ were discussed in Section 6 in the ESI.†

Origin of the hydrogen (deuterium) atoms in ammonia products

To investigate the mechanism of electrochemical ammonia formation, deuterium isotope analysis was conducted to determine the origin of hydrogen (deuterium) atoms in the ammonia products. The compositions of the ammonia products were determined using FTIR analysis. The flow rate over the

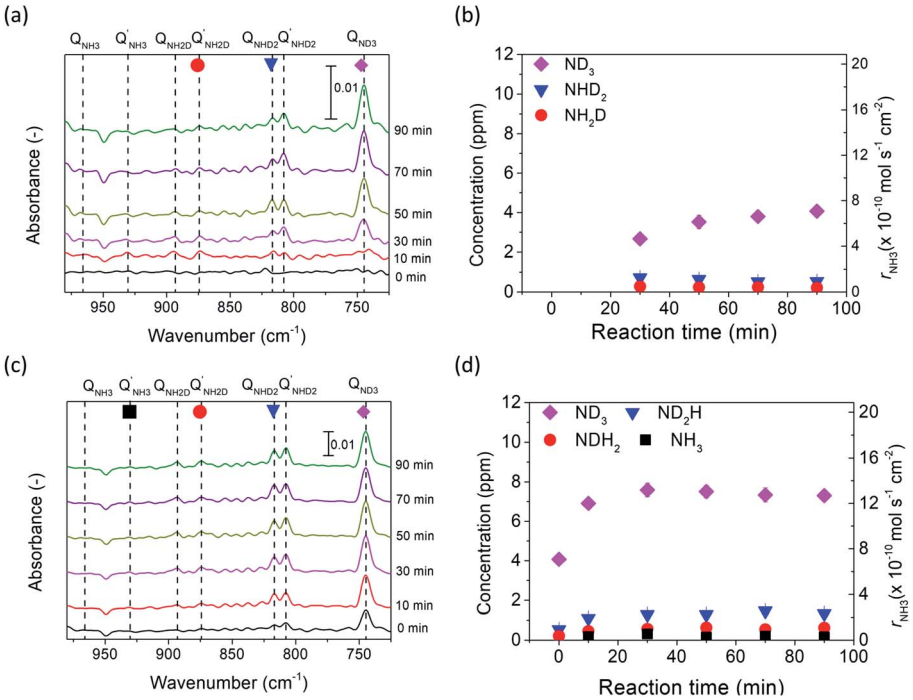

Fig. 5 (a) and (c) show the FTIR spectra of the ammonia product using porous pure Fe in 5% D_2–45% Ar–50% N_2 at rest potential and −1 V, respectively. (b) and (d) show the concentrations of $NH_{3-x}D_x$ in (a) and (c), respectively.

cathode was increased to 100 sccm in the FTIR analysis because of the large volume of the optical cell. The deuterium isotope analysis can be divided into three stages. In the first stage, valve 1 (Fig. S6†) was switched to flow the gaseous mixture into the FTIR cell, and valves 2 and 3 were opened. The cell operation conditions were maintained at 10% H_2–3% H_2O–87% Ar, Pt|BCY|Fe, 5% D_2–45% Ar–50% N_2 at 550 °C. Fig. 5a shows the FTIR spectra at rest potential, in which the peaks of ND_3, NHD_2, and NH_2D can be seen. Fig. 5b also shows the concentrations of ND_3, NHD_2, and NH_2D (the absorption coefficients of NH_3D_{3-x}

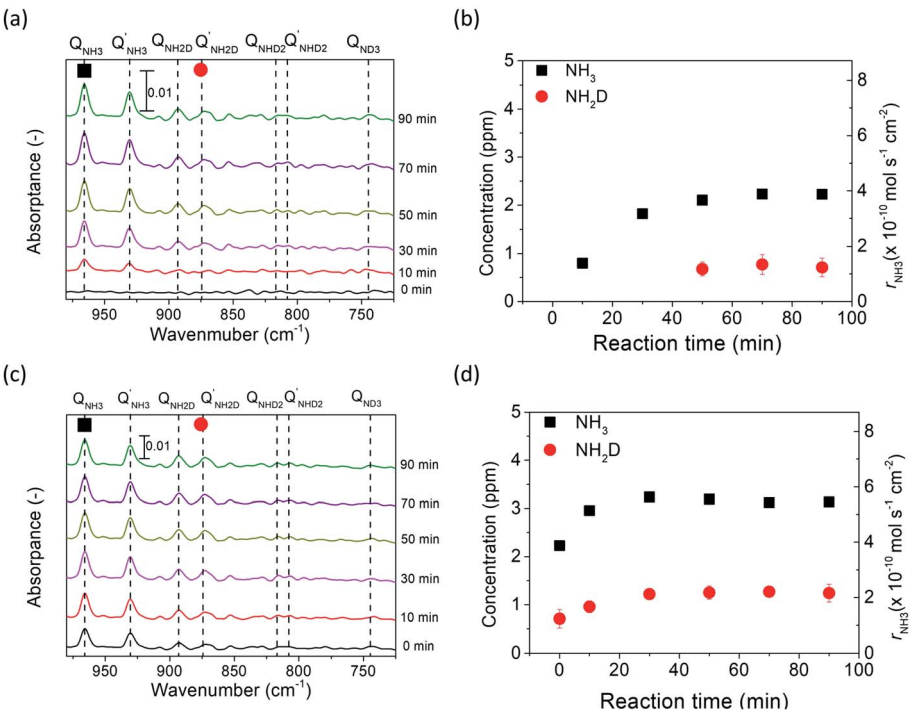

Fig. 6 (a) and (c) show the FTIR spectra of the ammonia product using porous pure Fe at 5% H_2–95% N_2 at rest potential and −1 V, respectively. (b) and (d) show the concentrations of the $NH_{3-x}D_x$ peaks in (a) and (c), respectively.

are discussed in Section 6 in the ESI†). The ammonia product should be ND_3 at the rest potential because H^+ cannot be supplied from the anode at the rest potential, whereas ND_3, NHD_2, and NH_2D were observed at the rest potential. The products NHD_2 and NH_2D were probably formed *via* exchange reactions with ND_3 and H_2O in the outlet, that is, in the quartz tube, gas tube, and optical cell (eqn (9) and (10)) or *via* the surface reaction with nitrogen atoms and some hydrogen atoms that had diffused from the anode to the cathode because of the H_2 concentration gradient (see Section 8 in the ESI†). H_2O may generate *via* H_2O release from hydroxide defects in BCY electrolyte. At the rest potential, the main composition of the ammonia was ND_3 *via* the surface reaction without cathodic polarization.

$$ND_3 + H_2O \rightarrow ND_2H + HDO \quad (9)$$

$$ND_2H + H_2O \rightarrow NDH_2 + HDO \quad (10)$$

In the second stage, a voltage of −1 V was applied to the cell to investigate the composition of the ammonia in the electrochemical reaction. All valves were set the same as those in the first stage. The intensities of the ND_3, NHD_2, and NH_2D peaks increased at −1 V, and a weak NH_3 peak was observed, as shown in Fig. 5c. The concentrations of $NH_{3-x}D_x$ are shown in Fig. 5d. In the second stage, the ammonia products were determined by the surface reaction, electrochemical reaction, and exchange reaction. The mechanism of the electrochemical ammonia formation reaction is discussed later.

In the third stage, valves 1, 2, and 3 were closed to examine the influence of the optical cell on the concentration of ammonia product (*i.e.*, the adsorption or decomposition of ammonia). The intensities of the ND_3 peaks monotonously decreased with elapsed time, whereas the intensities of the NH_3, NH_2D, and NHD_2 peaks did not change with elapsed time, as shown in Fig. S7.† Thus, the decrease in the ND_3 concentration was caused by the decomposition rather than the exchange reaction of ND_3 and H_2O to form $NH_{3-x}D_x$ in the optical cell. The decomposition rate was about 0.4% per min based on the result in the stage 3, and the space time in the optical cell was 5 min in the stage 2, considering the current condition (the total gas flow rate in the cathode:100 sccm; the volume of the optical cell: 500 cm^3). Therefore, the decomposition rate in the space time was around 2% in the stage 2, which can be negligible in our experiments.

Mechanism of electrochemical ammonia synthesis reaction

In the cell with 10% H_2–3% H_2O–87% Ar, Pt|BCY|Fe, 5% D_2–45% Ar–50% N_2, the main product was ND_3 at rest potential. After applying a voltage of −1 V, the ammonia formation rate increased, probably *via* the charge-transfer reaction or the surface reaction with EPOC. If the ammonia were formed by the charge-transfer reaction (faradaic reaction), in which N_2 reacts with H^+ from the anode, the product would be NH_3. The ammonia formation reactions were summarized in Table 2. The charge-transfer reactions are given by eqn (11a)–(13). On the other hand, if the ammonia were formed *via* the surface reaction with EPOC, in which N_2 reacts with D_2 at the cathode, the product would be ND_3 (eqn (11b) and (14)–(17)). If electrochemical ammonia formation is followed by the charge-transfer reaction, the main product should be NH_3 at −1 V. However, this assumption is not consistent with the fact that the main product was ND_3 at −1 V (Fig. 5d). After applying a voltage of −1 V, the concentration of ND_3 increased by approximately 3.5 ppm (4 → 7.5 ppm), whereas the concentrations of NHD_2, NH_2D, and NH_3 increased by approximately 0.8, 0.4, and 0.16 ppm, respectively. Therefore, in the second stage (*i.e.*, at −1 V), ND_3 is the main product in the electrochemical ammonia synthesis reaction, which indicates that electrochemical ammonia formation is mainly followed by the surface reaction with EPOC. In conclusion, in the electrochemical ammonia synthesis reaction, ammonia is formed *via* the surface reaction in the cathode rather than the charge-transfer reaction with cathodic polarization.

Table 2 Reaction steps of electrochemical ammonia formation for the two mechanisms

Charge-transfer reaction (faradaic reaction)		Surface reaction (EPOC)	
$N_2(g) + * \rightarrow N_2*$	(11a)	$N_2(g) + * \rightarrow N_2^*$	(11b)
$N_2^* + 3H^+ + 3e^- \rightarrow NH_3(g) + N*$	(12)	$N_2^* + * \rightarrow 2N*$	(14)
$N* + 3H^+ + 3e^- \rightarrow NH_3(g)$	(13)	$D_2(g) + 2* \rightarrow 2D*$	(15)
		$N* + 3D* \rightarrow ND_3^* + 3*$	(16)
		$ND_3^* \rightarrow ND_3(g) + *$	(17)

For the products of NHD_2, NH_2D, and NH_3, the H atoms in these three products were probably formed *via* three pathways: (1) the surface reaction with adsorbed N and H atoms, (2) the exchange reaction with H_2O, and (3) the charge-transfer reaction. If we assume that all H atoms are formed from the charge-transfer reaction, the current efficiency, η, can be obtained using eqn (18).

$$\eta = \frac{i_{NH_{3-x}D_x} \times F \times n}{i} = \frac{\left(c_{NH_{3-x}D_x,-1\ V} - c_{NH_{3-x}D_x,0}\right) \times 10^{-6} \times f \times F \times n}{R \times T \times A \times i} \quad (18)$$

where i_{NH_3-xDx}, $c_{NH_3-xDx,-1\ V}$, and $c_{NH_3-xDx,0}$ are the current density for ammonia formation, concentration of $NH_{3-x}D_x$ at −1 V, and concentration of $NH_{3-x}D_x$ at rest potential, respectively. Notably, the values of n were 3, 2, and 1 for NH_3, NH_2D, and NHD_2, respectively, because only H atoms form *via* the charge-transfer reaction. The obtained current efficiency is approximately 0.12%, which is very low for an electrochemical reaction. Thus, the charge-transfer reaction is not dominant in this case.

Deuterium isotope analysis on introducing H_2 into the cathode and D_2 into the anode

The deuterium isotope analysis was also conducted using 5% H_2–95% N_2 in the cathode and wet 10% D_2–90% Ar in the anode, and the results are shown in Fig. 6. The area of the NH_2D Q branch was determined by deconvoluting the overlapped

spectra between the NH_2D Q′ branch and the NH_3 P branch. Fig. S8† shows an example of the deconvoluted spectrum. In the first stage (*i.e.*, valves 1, 2, and 3 open), strong NH_3 peaks and small NH_2D peaks were observed at rest potential, and the concentrations of NH_3 and NH_2D were calculated, as shown in Fig. 6a and b. NH_3 was the main product formed by the surface reaction without cathodic polarization. The D atoms in NH_2D originated from the diffusion of D^+ from the anode (see Section 8 in the ESI†).

Then, in the second stage (valves 1, 2, and 3 open), the concentrations of NH_3 and NH_2D increased at an applied voltage of −1 V, as shown in Fig. 6c and d. Again, if electrochemical ammonia formation is followed by the charge-transfer reaction, the product will be ND_3. If the electrochemical ammonia formation is followed by the surface reaction, the product will be NH_3. The concentrations of NH_3 and NH_2D increased by approximately 0.9 and 0.5 ppm, respectively, which indicates that the main product was NH_3 formed *via* the surface reaction at −1 V. This result agrees with the former result of ND_3 formation at −1 V *via* the surface reaction. In the third stage (valves 2 and 3 closed), the intensities of NH_3 and NH_2D peaks did not change with time, as shown in Fig. S9.†

The dependence of the charge-transfer reaction on the applied voltage was also investigated using a cell of wet 10% D_2–90% Ar, Pt|BCY|Fe, H_2–N_2 at −0.3, −0.7, and −1 V, as shown in Fig. 7. This figure shows that the concentrations of NH_3 and NH_2D correspond to the H_2 and D^+ flow rates in the cathode, respectively. The H_2 flow rate used in Fig. 7a is defined as the H_2 partial pressure in the cathode. Hydrogen partial pressures of 3% and 5% correspond to H_2 flow rates of 5.1×10^{-6} and 8.7×10^{-6} mol cm^{-2} s^{-1}, respectively. When a voltage was applied, because only D^+ was pumped into the cathode, the H_2 partial pressure did not change with increasing current density. As shown in Fig. 7b, the D_2 partial pressure is defined as the sum of the D_2 partial pressure caused by the D_2 evolution reaction and D_2 diffusion from the anode. Therefore, the D_2 partial pressure increased with increasing current density.

As shown in Fig. 7a, 2.2 ppm NH_3 was detected in 5% H_2 at rest potential. When a voltage was applied, the concentration of NH_3 increased to 2.5–3.1 ppm at different applied voltages, although the H_2 partial pressure remained the same at 5%. When the H_2 partial pressure in the cathode decreased to 3%, NH_3 concentration also decreased to 1.3 ppm at the rest potential and increased to 1.4–1.6 ppm at different applied voltages. Because the H_2 partial pressure does not change, this result suggests that the increase in NH_3 concentration is caused by the EPOC, and that the effect of the EPOC on the ammonia formation rate depends on the applied voltage and the H_2 partial pressure in the cathode.

As shown in Fig. 7b, some D_2 diffused from the anode to the cathode at the rest potential. Based on the calculation of D_2 diffusion through the electrolyte, the D_2 partial pressure was 7.6×10^{-7} atm at the rest potential (see Section 8 in the ESI†). NH_2D was formed *via* the surface reaction with H_2, D_2, and N_2 at the rest potential. When a voltage was applied (−0.3 to −1.0 V), the D_2 partial pressure increased with increasing current density because of the increase in the pumping of D^+ cations

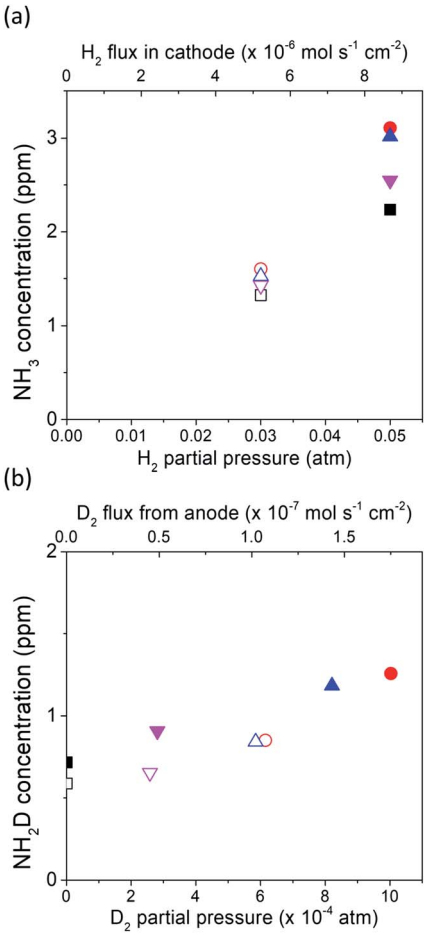

Fig. 7 (a) Concentration of NH_3 at rest potentials of −0.3, −0.7, and −1 V in 5% H_2–95% N_2 and 3% H_2–97% N_2. (b) Concentration of NH_2D at rest potentials of −0.3, −0.7, and −1 V in 5% H_2–95% N_2 and 3% H_2–97% N_2. Because of the flux of D^+ from the anode into the cathode with cathode polarization, the H_2 flux did not change with cathodic polarization and the D_2 flux increased with increasing current density. ■ 5% H_2–95% N_2 at rest potential. □ 3% H_2–97% N_2 at rest potential. ● 5% H_2–95% N_2 at −1 V. ○ 3% H_2–97% N_2 −1 V. ▲ 5% H_2–95% N_2 at −0.7 V. △ 3% H_2–97% N_2 at −0.7 V. ▼ 5% H_2–95% N_2 at −0.3 V. ▽ 3% H_2–97% N_2 at −0.3 V.

(*i.e.* increase in current density), and the NH_2D concentration increased with increasing applied voltage as well. However, the D^+ flux at the applied voltage was hundreds of times larger than that at the rest potential, whereas the NH_2D concentration only increased by approximately 29%–68%, which suggests that an increase in the D^+ flux (*i.e.*, current density) cannot promote the charge-transfer reaction.

In general, increasing the ammonia concentration in the electrochemical reaction involves three reactions: (1) the EPOC effect, (2) promotion of the surface reaction because of increase in D^+ diffused from the anode to the Fe surface (*i.e.*, thermal reaction of D atoms with N*), and (3) charge-transfer reaction of $N^* + D^+ + e^- \rightarrow ND^*$. To understand the contribution of the charge-transfer reaction, we made two assumptions: (1) the exchange reaction (*e.g.*, $NH_3 + D_2 \rightarrow NH_2D + HD$) is negligible in this system and (2) all D atoms in NH_2D originate from the

charge-transfer reaction. Therefore, the current efficiency, which can be obtained by eqn (19) with $n = 1$ for NH_2D, was approximately 0.01% to 0.06%, suggesting low ammonia formation from the charge-transfer reaction. Based on deuterium isotope analysis, the main product of ammonia originates from H_2 (or D_2) in the cathode. The low current efficiency suggests a low contribution of the charge-transfer reaction. Under practical conditions, H_2–Ar and H_2–N_2 are introduced into the cathode and anode, respectively. If we assume that the current efficiency is approximately 0.1% and that the current efficiency does not change with H_2 partial pressure in the cathode, the ammonia formation rate at −1.3 V in Fig. 4a can be divided into the ammonia formation rate from (a) the EPOC: $r_{NH_3,EPOC}$, (b) charge-transfer reaction: $r_{NH_3,CT}$, (obtained by eqn (19)), and (c) surface reaction at rest potential: $r_{NH_3,0}$, as shown in Fig. 8. The values of total ammonia formation rate, $r_{NH_3,total}$, and $r_{NH_3,0}$, were obtained in Fig. 8. Therefore, $r_{NH_3,EPOC}$ can be obtained by eqn (19):

$$r_{NH_3,EPOC} = r_{NH_3,total} - r_{NH_3,0} - r_{NH_3,CT} \quad (19)$$

Notably, the ammonia concentration from the charge-transfer reaction was around 2.5 ppm at different H_2 partial pressures, whereas the ammonia concentration originating from the EPOC increased from 3.0 ppm in 5% H_2–50% N_2–45% Ar to 40.2 ppm in 25% H_2–50% N_2–25% Ar at −1.3 V. This result indicates that the EPOC contribution can be significantly improved by increasing the H_2 partial pressure in the cathode.

The results are summarized as follows: (1) the ammonia formation rate has a positive correlation with H_2 partial pressure in the cathode, which agrees with the previous study.[38] (2) α and β do not change after applying different voltages, which indicates that the reaction mechanism is probably the same as that at the rest potential (surface reaction). (3) The contribution of surface reaction with EPOC to ammonia formation rate is larger than that of charge-transfer reaction with porous pure Fe, and the ammonia formation rate promoted by EPOC can be improved by increasing H_2 partial pressure in the cathode. The results reveal an alternative route, *i.e.*, surface reaction with EPOC, for electrochemical ammonia formation. Based on our previous study,[38] we believe that the effect of the EPOC is probably induced by the formation of an effective double layer *via* the spillover of proton originating from charge carriers in the electrolyte to promote the reaction of ammonia formation. Our findings will aid in the design of new catalyst structures for the electrochemical synthesis of ammonia.

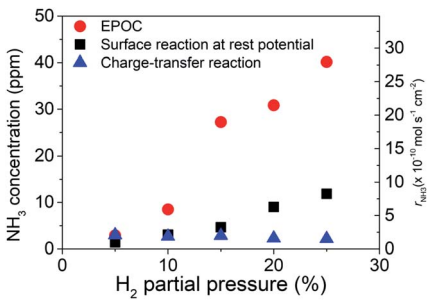

Fig. 8 NH_3 concentrations at −1.3 V and different H_2 partial pressures.

Conclusions

In this study, the mechanism of electrochemical ammonia formation with a porous pure Fe cathode catalyst at 550 °C was investigated by kinetic and deuterium isotope analyses. The ammonia formation rate increased with increasing the applied negative voltage and with increasing the H_2 partial pressure in the cathode. The reaction orders for hydrogen, α, and nitrogen, β, did not change at different applied negative voltages, which indicates that the mechanism of ammonia formation at rest potential was the same as that at an applied negative voltage. Further, the origin of electrochemical ammonia formation, EPOC or faradaic reaction, was investigated by deuterium isotope analysis. The main ammonia product (NH_3 or ND_3) corresponded to the hydrogen/deuterium species in the cathode, suggesting that the surface reaction with EPOC is dominant in the electrochemical ammonia formation reaction. In addition, the effect of the EPOC on ammonia formation depends on the applied voltage and hydrogen partial pressure. However, the contribution of the charge-transfer reaction to ammonia formation was relatively small. The results of this study will contribute to the design of cathode structures for electrochemical ammonia formation.

Experimental

Powder fabrication

The coprecipitation method was used to prepare $BaCe_{0.9}Y_{0.1}O_3$ (BCY) powder from the precursors $Ba(NO_3)_2$ (purity: 99.99%, Kanto Chemical Co., Inc., Japan), $Ce(NO_3)_3 \cdot 6H_2O$ (purity: 99.99%, Kanto Chemical Co., Inc., Japan), and $Y(NO_3)_3 \cdot 6H_2O$ (purity: 99.99%, Kanto Chemical Co., Inc., Japan). These precursors were stoichiometrically dissolved in 300 mL ultrapure water (Autopure WT 100, Yamato, Scientific Co., Ltd, Japan), and $(NH_4)_2(COO)_2$ (purity: 99.5%, Kanto Chemical Co. Inc., Japan), whose concentration was 1.5 times higher than the total cation concentration, was dissolved in 600 mL ultrapure water. The precursor solution was slowly added to the $(NH_4)_2(COO)_2$ solution to form a white precipitate. The mixture was then filtered using suction filtration and dried at 80 °C for one day. The dried powder was precalcined at 800 °C and then calcined at 1200 °C in air to yield the BCY powder.

Cell fabrication

BCY pellets were prepared by uniaxial pressing and subsequent cold isostatic pressing. BCY powder (1.5 g) was first uniaxially pressed at a pressure of 1 t cm^{-2} and then, isostatically pressed at 180 MPa. The BCY pellet was then calcined at 1600 °C for 5 h in air with sacrificial BCY powder to prevent intermixing with the crucible and the vaporization of barium.

A porous Fe electrode was prepared on a BCY electrolyte using the doctor-blade method. The Fe_2O_3 powder was mixed

with a gel composed of α-terpineol (solvent) (purity: 98%, Fujifilm Wako Pure Chemical, Co., Inc., Japan), ethyl cellulose (binder) (ethoxy content: 48.0. −49.5%, Kanto Chemical, Co., Inc., Japan), NONION OP-83 RAT sorbitan sesquioleate (dispersant) (NOF, Co., Japan), dibutyl phthalate (plasticizer) (purity: 99.5%, Kanto Chemical, Co., Inc., Japan), and poly(-methylmethacrylate) resin (pore formation) (purity: 99.9%, Tokyo Chemical Industry, Co., Ltd., Japan) to form a slurry. The slurry was then pasted onto the BCY electrolyte and calcined at 900 °C in air to obtain the porous pure Fe_2O_3 electrode on the BCY electrolyte. Then, Pt counter electrode and Pt reference electrode were pasted on the backside of BCY electrolyte by the doctor blade method. The obtained sample was then reduced at 900 °C for 1 h in 3% H_2 to obtain a porous pure Fe cathode, as shown in Fig. S10.†

Characterizations

The samples were characterized using scanning electron microscopy (SEM, S4700 Hitachi and JSM-7900F JEOL, Japan) and X-ray diffractometry (XRD, SmartLab, RIGAKU, Japan).

Electrochemical synthesis of ammonia

An electrolyte-supported cell was set in between two quartz tubes in a furnace, as shown in Fig. S6.† Pyrex glass rings were used to seal the quartz tubes at 900 °C. After sealing, Fe cathode was reduced in 3% H_2–97% Ar at 900 °C. Then, the temperature was lowered to 550 °C. The electrosynthesis of ammonia was carried out at 550 °C using cells containing 20% H_2–3% H_2O–77% Ar (30 standard cubic centimeters (sccm)), Pt|BCY|Fe, N_2–H_2–Ar. The reaction conditions are summarized in Table S11.† Potentiostatic and alternating current (AC) impedance measurements were performed from 1 to 10^6 Hz using an Autolab PGSTAT128N (Metrohm Autolab B.V., Netherlands). The ammonia formation rate was measured by flowing the outlet gas into a 0.01 mM H_2SO_4 capture solution, which was prepared by using ultrapure water (100 mL) (Autopure WT 100 compatible with Milli-Q, Yamato Scientific Co., Ltd., Japan) and 0.005 M H_2SO_4 solution (0.1 mL) (Kanto Chemical, Co., Inc., Japan), for 5 min. Then, the capture solution was subsequently analysed using high-performance ion chromatography (HPLC) (EXTREMA, Jasco, Japan). The ammonia formation rate (r_{NH3}) was calculated using eqn (20).

$$r_{NH_3} = \frac{\left[NH_4^+\right] \times V}{t \times A} \quad (20)$$

Here, $[NH_4^+]V$, t, and A are the NH_4 ion concentration measured by HPLC, volume of the H_2SO_4 capture solution, capture time, and electrode area (*ca.* 39.3 mm^2), respectively. The composition of the produced ammonia was analyzed by flowing the outlet gas into an FTIR device (FT/IR 670 Plus, JASCO, Japan) with a cell having a long optical path length (LPC-8M-S, JASCO, Japan), as shown in Fig. S6.† The gas-line (SUS316) connecting the electrochemical equipment and FTIR was kept at 80 °C and the optical cell was kept at 70 °C to prevent ammonia from adsorbing on the surface in the gas tubes and the optical cell. In addition, to examine the influence of contamination on kinetic and deuterium isotope analyses, we conducted the experiments according to the protocol for benchmarking of ammonia electrochemical synthesis, which was shown in Sections 14–18 in the ESI.†

Author contributions

Chien-I Li: writing-original draft preparation, investigation, formal analysis. Hiroki Matsuo: methodology, data curation, validation. Junichiro Otomo: conceptualization, methodology, writing – reviewing and editing, data curation, supervision.

Conflicts of interest

The authors declare no conflict of interest.

Acknowledgements

The authors thank CREST, Japan Science and Technology Agency (JPMJCR1441) for financial support; the Materials Design and Characterization Laboratory, Institute for Solid State Physics, The University of Tokyo for use of the SEM and XRD facilities.

References

1 D. Bernhardt and J. F. Reilly II, *U. S. Geological Survey*, U.S. Government Publishing Office, Washington DC, 2019, p. 118.
2 J. W. Erisman, M. A. Sutton, J. Galloway, Z. Klimont and W. Winiwarter, *Nat. Geosci.*, 2008, **1**, 636–639.
3 S. Giddey, S. P. S. Badwal, C. Munnings and M. Dolan, *ACS Sustainable Chem. Eng.*, 2017, **5**, 10231–10239.
4 W. Wang, J. M. Herreros, A. Tsolakis and A. P. E. York, *Int. J. Hydrogen Energy*, 2013, **38**, 9907–9917.
5 F. Hayashi, Y. Toda, Y. Kanie, M. Kitano, Y. Inoue, T. Yokoyama, M. Hara and H. Hosono, *Chem. Sci.*, 2013, **4**, 3124.
6 M. Appl, *Ammonia principles and industrial practice*, Wiley-VCH, Germany, 1999.
7 H. Liu, *Ammonia Synthesis Catalysts Innovation and Practice*, World Scientific, 2013.
8 A. Ozaki and H. Taylor, *Proc. R. Soc. London, Ser. A*, 1960, **258**(1292), 47–62.
9 K.-I. Aika, H. Hori and A. Ozaki, *J. Catal.*, 1972, **27**, 424–431.
10 M. Kitano, Y. Inoue, Y. Yamazaki, F. Hayashi, S. Kanbara, S. Matsuishi, T. Yokoyama, S. W. Kim, M. Hara and H. Hosono, *Nat. Chem.*, 2012, **4**(11), 934–940.
11 M. Kitano, S. Kanbara, Y. Inoue, N. Kuganathan, P. V. Sushko, T. Yokoyama, M. Hara and H. Hosono, *Nat. Commun.*, 2015, **6**, 6731.
12 J. N. Renner, L. F. Greenlee, A. M. Herring and K. E. Ayers, *Electrochem. Soc. Interface*, 2015, **24**(2), 51–57.
13 E. Skulason, T. Bligaard, S. Gudmundsdottir, F. Studt, J. Rossmeisl, F. Abild-Pedersen, T. Vegge, H. Jonsson and J. K. Norskov, *Phys. Chem. Chem. Phys.*, 2012, **14**, 1235–1245.

14 S. Zhang, G. Duan, L. Qiao, Y. Tang, Y. Chen, Y. Sun, P. Wan and S. Zhang, *Industrial & Engineering Chemistry Research*, 2019.
15 S. Luo, X. Li, B. Zhang, Z. Luo and M. Luo, *ACS Appl. Mater. Interfaces*, 2019, **11**, 26891–26897.
16 R. Liu and G. Xu, *Chin. J. Chem.*, 2010, **28**, 139–142.
17 G. Xu, R. Liu and J. Wang, *Sci. China, Ser. B: Chem.*, 2009, **52**(8), 1171–1175.
18 V. Kordali, G. Kyriacou and C. Lambrou, *Chem. Commun.*, 2000, 1673–1674.
19 R. Lan, J. T. Irvine and S. Tao, *Sci. Rep.*, 2013, **3**, 1145.
20 Z. Zhang, Z. Zhong and R. Liu, *J. Rare Earths*, 2010, **28**(4), 556–559.
21 M. Wang, S. Liu, T. Qian, J. Liu, J. Zhou, H. Ji, J. Xiong, J. Zhong and C. Yan, *Nat. Commun.*, 2019, **10**, 341.
22 Z. Li, R. Liu, Y. Xie, S. Feng and J. Wang, *Solid State Ionics*, 2005, **176**(11–12), 1063–1066.
23 A. Skodra and M. Stoukides, *Solid State Ionics*, 2009, **180**(23–25), 1332–1336.
24 D. S. Yun, J. H. Joo, J. H. Yu, H. C. Yoon, J.-N. Kim and C.-Y. Yoo, *J. Power Sources*, 2015, **284**, 245–251.
25 F. Kosaka, T. Nakamura and J. Otomo, *J. Electrochem. Soc.*, 2017, **164**(13), F1323–F1330.
26 N. Shimoda, Y. Kobayashi, Y. Kimura, G. Nakagawa and S. Satokawa, *J. Ceram. Soc. Jpn.*, 2017, **125**, 252–256.
27 J. Otomo, N. Noda and F. Kosaka, *ECS Trans.*, 2015, **68**, 2663–2670.
28 F. Kosaka, N. Noda, T. Nakamura and J. Otomo, *J. Mater. Sci.*, 2016, **52**, 2825–2835.
29 Z.-J. Li, R.-Q. Liu, J.-D. Wang, Y.-H. Xie and F. Yue, *J. Solid State Electrochem.*, 2004, **9**(4), 201–204.
30 Y.-H. Xie, J.-D. Wang, R.-Q. Liu, X.-T. Su, Z.-P. Sun and Z.-J. Li, *Solid State Ionics*, 2004, **168**(1–2), 117–121.
31 F. Zhang, Q. Yang, B. Pan, R. Xu, H. Wang and G. Ma, *Mater. Lett.*, 2007, **61**(19–20), 4144–4148.
32 J.-D. Wang, Y.-H. Xie, Z.-F. Zhang, R.-Q. Liu and Z.-J. Li, *Mater. Res. Bull.*, 2005, **40**(8), 1294–1302.
33 H. Kim, Y. S. Chung, T. Kim, H. Yoon, J. G. Sung, H. K. Jung, W. B. Kim, L. B. Sammes and J. S. Chung, *Solid State Ionics*, 2019, **339**, 115010.
34 E. Vasileiou, V. Kyriakou, I. Garagounis, A. Vourros, A. Manerbino, W. G. Coors and M. Stoukides, *Solid State Ionics*, 2016, **288**, 357–362.
35 M. Ouzounidou, A. Skodra, C. Kokkofitis and M. Stoukides, *Solid State Ionics*, 2007, **178**(1–2), 153–159.
36 E. Vasileiou, V. Kyriakou, I. Garagounis, A. Vourros and M. Stoukides, *Solid State Ionics*, 2015, **275**, 110–116.
37 F. Kosaka, T. Nakamura, A. Oikawa and J. Otomo, *ACS Sustainable Chem. Eng.*, 2017, **5**, 10439–10446.
38 C.-I. Li, H. Matsuo and J. Otomo, *Sustainable Energy Fuels*, 2021, **5**, 188–198.
39 S. Z. Andersen, V. Colic, S. Yang, J. A. Schwalbe, A. C. Nielander, J. M. McEnaney, K. Enemark-Rasmussen, J. G. Baker, A. R. Singh, B. A. Rohr, M. J. Statt, S. J. Blair, S. Mezzavilla, J. Kibsgaard, P. C. K. Vesborg, M. Cargnello, S. F. Bent, T. F. Jaramillo, I. E. L. Stephens, J. K. Norskov and I. Chorkendorff, *Nature*, 2019, **570**, 504–508.
40 R. Kojima and K.-i. Aika, *Appl. Catal., A*, 2001, **218**, 121–128.
41 C. W. David, *J. Chem. Educ.*, 1996, **73**(1), 46–50.